Chinese Journal of
POLYMER SCIENCE

RESEARCH ARTICLE

https://doi.org/10.1007/s10118-026-3876-2
Chinese J. Polym. Sci.

Crystallization, Brill Transition, and Physical Properties of Biobased 1,4-Butanediamine-derived Polyamides Controlled by Methylene Sequence Length

Jun-Jian Qiu[a,b], Ying Zheng[a,b*], Mao-Lin Li[b], Chang Zeng[b], Feng Zhou[c], Xian-Ming Li[d], Ke-Yuan Liu[d], Jun-Feng Liu[a,b], Cheng-Tao Yu[a,b], and Peng-Ju Pan[a,b*]

[a] *Institute of Zhejiang University-Quzhou, Polytechnic Institute of Zhejiang University, Quzhou 324000, China*
[b] *State Key Laboratory of Chemical Engineering and Low-Carbon Technology, Key Laboratory of Biomass Chemical Engineering of Ministry of Education, College of Chemical and Biological Engineering, Zhejiang University, Hangzhou 310058, China*
[c] *SINOPEC Dalian Research Institute of Petroleum and Petrochemicals Co., Ltd., Dalian 116045, China*
[d] *Jiangsu Qingquan Chemical Co., Ltd., Yancheng 224555, China*

Electronic Supplementary Information

Abstract The development of high-performance bio-based polyamides requires a molecular-level understanding of how the repeat-unit structure influences crystallization and macroscopic properties. Herein, a series of bio-based polyamides (denoted as PA4X) with different methylene sequence lengths were synthesized from 1,4-diaminobutane and aliphatic diacids. The crystallization behavior, crystalline phase transition, mechanical properties, and water absorption properties of PA4X were systematically investigated. The crystallization and melting temperatures, enthalpies, and crystallinity progressively decreased with increasing carbon numbers in the diacid monomer (*X*). All solution-crystallized PA4X form a triclinic *α* phase and undergo a reversible *α*-*γ* Brill transition during heating and cooling. The *α*-to-*γ* transition temperature depends strongly on the methylene sequence length and decreases from 253 °C to 203 °C as *X* increases from 6 to 12. Shorter-spaced PA4X exhibits higher stiffness, strength, and water absorption, whereas their longer-spaced analogs exhibit enhanced ductility and lower water absorption. This study establishes the structure-property relationships of PA4X polyamides and provides guidance for designing bio-based polyamides with tunable thermal, mechanical, and moisture-resistance performances.

Keywords Biobased polyamide; 1,4-Butanediamine; Crystallization behavior; Brill transition; Physical properties

Citation: Qiu, J. J.; Zheng, Y.; Li, M. L.; Zeng, C.; Zhou, F.; Li, X. M.; Liu, K. Y.; Liu, J. F.; Yu, C. T.; Pan, P. J. Crystallization, Brill transition, and physical properties of biobased 1,4-butanediamine-derived polyamides controlled by methylene sequence length. *Chinese J. Polym. Sci.* https://doi.org/10.1007/s10118-026-3876-2

INTRODUCTION

Polyamides constitute an important class of semicrystalline engineering polymers owing to their excellent mechanical strength, thermal resistance, chemical durability, and melt processability.[1,2] These properties have enabled their widespread use in fibers, electrical and electronic components, and other engineering applications. However, most commercial polyamides are currently produced from fossil-derived monomers.[3,4] Growing concerns regarding fossil resource depletion and the environmental impact of persistent plastic waste have intensified the demand for polymer materials derived from renewable feedstocks.[5,6]

Aliphatic polyamides are generally composed of alternating polar amide groups and nonpolar methylene sequences.[7,8] Variation in the methylene sequence length provides a direct means for regulating the amide-group density, intermolecular H-bonding, and segmental flexibility of the resulting polyamides. Previous studies on aliphatic polyamides have demonstrated that increasing the methylene sequence length in diacid units weakens intermolecular H-bonding and retards the crystallization of odd-even PA5X polyamides.[9] Similarly, in even-even long-spaced polyamides ranging from PA614 to PA618, an increase in the methylene sequence length decreased the H-bond density, promoted a transition from relatively brittle to more ductile mechanical behavior, and markedly reduced water absorption.[10] These progresses demonstrate that the methylene sequence length is a key structural parameter governing the crystallization behavior and macroscopic properties of aliphatic polyamides.

* Corresponding authors, E-mail: yzheng1@zju.edu.cn (Y.Z.)
E-mail: panpengju@zju.edu.cn (P.J.P.)
Special Topic: Celebrating the 130th Anniversary of Zhejiang University
Received August 1, 2026; Accepted September 7, 2026; Published online November 18, 2026

© Chinese Chemical Society
Institute of Chemistry, Chinese Academy of Sciences

The influence of methylene sequence length on thermal and mechanical behavior is highly correlated with the crystalline structure of polyamides, as both the H-bond organization and methylene segment conformation play decisive roles in crystalline packing. Aliphatic polyamides generally exhibit pronounced crystal polymorphism, among which the triclinic or monoclinic *α* phase and pseudohexagonal *γ* phase are the most frequently observed crystalline forms.[11–13] The *α* phase adopts more extended chain conformations and anisotropically packed H-bonded sheets, whereas the *γ* phase exhibits more symmetric pseudohexagonal packing and greater conformational disorder.[14–16] Upon heating, the *α* phase can transform into the *γ* phase, as manifested by the gradual convergence of two characteristic diffraction peaks into a single peak. This thermally induced crystal transition is commonly referred to as Brill transition.[17,18] The phase transition involves changes in the conformation of the methylene segment, H-bond organization, and lateral crystal packing within the crystal lattice.[19–22] The Brill transition can be regulated by both molecular structure[23,24] and crystallization conditions.[25,26] For the long-chain polyamide PA1012, Wang *et al.*[25] established a positive correlation between the degree of crystal perfection and the Brill transition temperature (T_B), and found that rapid cooling from the melt produced crystals with a lower crystal perfection index and a greater fraction of randomly distributed H-bonds, thereby leading to a lower T_B. In addition, chemical modification can also alter T_B by disturbing chain regularity, H-bond organization, and crystalline packing.[27,28]

1,4-Butanediamine (BDA), also known as putrescine, is particularly attractive because it can be produced *via* microbial fermentation and used as a renewable building block for the synthesis of bio-based polyamides.[29–31] Polycondensation of BDA with various aliphatic diacids provides a versatile molecular platform for constructing bio-based aliphatic polyamides with tunable chain structures and material properties. Accordingly, BDA-based polyamides, denoted PA4X, represent an important family of bio-based polyamides. Among them, PA46 and PA410 have already been industrialized and commercialized.[32,33] PA46 exhibits high crystallinity, excellent thermal resistance, and a relatively high T_B in the range of 180–250 °C.[17] In contrast, PA410 provides a favorable balance between mechanical strength, melt processability, and low moisture uptake.[34,35] Despite these advances, a systematic understanding of how the diacid structure regulates the crystallization, Brill transition, and physical performance of PA4X remains elusive.

Herein, a series of PA4X with distinct methylene sequence lengths was synthesized through aqueous prepolymerization followed by either solid-state or melt post-polycondensation. The post-polycondensation conditions were optimized to obtain a high-molecular-weight PA4X. Crystallization behavior, crystalline phase transition, mechanical properties, and water absorption were systematically investigated. We found that all PA4X samples underwent a reversible Brill transition upon heating and cooling, and T_B decreased gradually as the methylene sequence length in the diacid units increased. Furthermore, the dependence of the mechanical properties and water absorption on the methylene sequence length was elucidated.

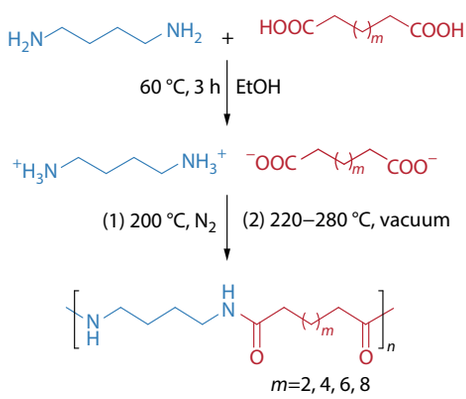
EXPERIMENTAL

Materials

Bio-based 1,4-diaminobutane (BDA) was purchased from China Resources Double Crane Pharmaceutical Co., Ltd. Adipic acid, suberic acid, sebacic acid, dodecanedioic acid, and formic acid were purchased from Shanghai Macklin Biochemical Co., Ltd. Deuterated sulfuric acid (D_2SO_4) was purchased from Shanghai Aladdin Biochemical Technology Co., Ltd. Ethanol was purchased from Sinopharm Group Co., Ltd. All the reagents were used as received without further purification.

Synthesis of BDA-based Polyamides

The BDA-based polyamides are denoted as PA4X, where *X* represents the carbon number of the diacid monomer used (*X*=6–12). The synthesis of PA4X comprised three main steps: nylon-salt formation, aqueous pre-polymerization, and post-polycondensation, as illustrated in Scheme 1. First, the corresponding nylon salts were prepared to achieve accurate stoichiometric control of the diamine and diacid functionalities during the polymerization. 0.5 mol% excess diamine was added to maintain the stoichiometric balance to compensate for the loss of volatile BDA during salt preparation and polycondensation. Diamine and diacid were dissolved separately in ethanol at 60 °C under continuous stirring. After complete dissolution, the diamine solution was added slowly to the diacid solution, resulting in a white precipitate. The mixture was subsequently cooled to 25 °C, and the precipitated nylon salt was collected by filtration, thoroughly washed with ethanol to remove impurities, and then dried under vacuum.



Scheme 1 Synthetic route of PA4X.

The resulting nylon salt was dissolved in deionized water to prepare a 50 wt% aqueous salt solution without adding antioxidants, which was then transferred to a 250 mL high-pressure reactor. The reactor was purged thrice with high-purity nitrogen at room temperature to remove residual air, after which an initial nitrogen pressure of 0.5 MPa was retained. The reactor mixture was heated to 200 °C and stirred at this temperature for 2 h for prepolymerization. Subsequently, water vapor was gradually released from the reactor and the pressure was slowly reduced to atmospheric pressure.

Different post-polycondensation procedures were used for PA4X. Solid-state post-polycondensation (SSP) was used for

https://doi.org/10.1007/s10118-026-3876-2

PA46 and PA48 because of its high melting temperature (T_m). After completion of the aqueous prepolymerization, the reactor was depressurized to atmospheric pressure and cooled to room temperature. The prepolymer was removed, pulverized into a powder, and then subjected to SSP under vacuum at 220–270 °C for 8–16 h. In contrast, melt post-polycondensation (MP) was employed for PA410 and PA412 because of their lower T_m. After the pressure was reduced to atmospheric pressure, the temperature was increased to 270 °C and the reaction was continued under vacuum for 6–8 h. After polymerization, the crude product was purified by complete dissolution in formic acid without observable gelation and subsequently precipitated into excess deionized water. The precipitated polymer was collected by filtration, thoroughly washed with deionized water, and dried under vacuum at 60 °C for 24 h. The yield of the synthesized PA4X was about 85%.

To prepare the solution-crystallized samples, purified polyamides were dissolved in formic acid at 60 °C to obtain solutions with a concentration of 10 g/L. The homogeneous solution was then poured into Teflon dishes and allowed to evaporate at room temperature for 48 h. The obtained samples were further dried under vacuum at 40 °C for 24 h to remove the residual solvent completely.

Characterizations

Nuclear magnetic resonance (NMR) spectroscopy

^{1}H-NMR spectra were recorded on a Bruker Avance NEO 500 MHz NMR spectrometer (Bruker, Germany) at 25 °C. The samples were dissolved in deuterated sulfuric acid (D_2SO_4) at a concentration of 20 mg/mL for ^{1}H-NMR analysis.

Intrinsic viscosity

Intrinsic viscosity (η) of the polyamides was measured using an Ubbelohde viscometer at 25 °C, using 90 wt% formic acid aqueous solution as the solvent and employing a polymer concentration of 0.005 g/mL. The η value was calculated as $[2(\eta_{sp}-\ln\eta_r)]^{0.5}/c$, where η_r is the relative viscosity, η_{sp} is the specific viscosity, and c is the mass concentration of polyamide (g/L).

Thermogravimetric analysis (TGA)

TGA was performed using a TGA Q500 instrument (TA, USA). The sample (about 3 mg) was heated from 25 °C to 600 °C at 10 °C/min under a nitrogen purge (50 mL/min) in the TGA.

Differential scanning calorimetry (DSC)

The crystallization and thermal behaviors of the polyamides were measured using a Netzsch 214 Polyma DSC instrument (Netzsch, Germany) equipped with an IC70 cooler under a nitrogen gas flow of 40 mL/min. The non-isothermal crystallization and melting behavior of the sample (6–8 mg) was conducted in a sealed aluminum pan according to the following procedure: (1) heating from 20 °C to 320 °C at 10 °C/min and holding at 320 °C for 5 min to erase the thermal history; (2) cooling to −30 °C at 10 °C/min to investigate the non-isothermal crystallization behavior; and (3) reheating to 320 °C at 10 °C/min to analyze the subsequent melting behavior.

Wide- and small-angle X-ray scattering (WAXS/SAXS)

WAXS analyses were conducted on a Nano-inXider vertical WAXS/SAXS system (Xenocs, France) equipped with two semiconductor pixel detectors (Pilatus 100 K for WAXS and Pilatus 200 K for SAXS; Dectris, Switzerland). The X-ray wavelength was set to 0.154 nm. The sample-to-detector distances were 79 and 936 mm for the WAXS and SAXS measurements, respectively. For temperature-variable WAXS measurements, the solution-crystallized sample sandwiched between aluminum foils was heated from 25 °C to the melt state and then cooled to 25 °C at 5 °C/min on a Linkam HFSX350 hot stage (Linkam Scientific Instruments, UK), during which the WAXS pattern was collected at 3 min interval.

Uniaxial tensile testing

Uniaxial tensile tests were performed using a universal testing machine (SUNS UTM4203, China) with a crosshead speed of 10 mm/min at 25 °C. The dumbbell-shaped specimens (15 mm in length, 3.0 mm in cross-section width, and 0.5 mm in thickness) were cut from the hot-pressed polyamide sheets. The yield stress, Young's modulus, and strain at break were derived from the engineering stress-strain curves. Five measurements were performed for each sample, and the average results were used.

Water absorption

The sample was hot-pressed into a square specimen of dimensions 60 mm × 60 mm × 1 mm. Before testing, the specimen was dried under vacuum at 50 °C for 24 h until a constant weight was reached. The initial dry weights were recorded as W_0. The specimens were then immersed in deionized water at 23 °C. At predetermined time intervals, the specimen was removed from the water and the surface water was carefully removed with clean and dry tissue within 1 min. The weight of the wet specimen (W_t) was recorded at certain intervals until the weight no longer changed. The water absorption (W) was calculated according to $W = (W_t - W_0)/W_0 \times 100\%$.

RESULTS AND DISCUSSION

Synthesis and Structural Characterization of Polyamides

BDA-based PA4X polyamides, including PA46, PA48, PA410, and PA412, were synthesized by aqueous prepolymerization followed by either solid-state post-polycondensation (SSP) or melt post-polycondensation (MP), as illustrated in Scheme 1. To establish suitable post-polycondensation conditions for PA4X, PA46 and PA412 were selected as representative systems to investigate the variation in intrinsic viscosity with reaction time and temperature under the SSP and MP conditions, respectively (Fig. 1). The PA46 prepolymer used in the SSP experiment had an intrinsic viscosity of 0.23 dL/g. As shown in Fig. 1(a), the intrinsic viscosity of PA46 increased continuously with both SSP temperature and reaction time. At each temperature, the intrinsic viscosity increased rapidly during the initial stage and subsequently plateaued, indicating a progressive decrease in the polycondensation rate as the reaction proceeded. Increasing the SSP temperature from 230 °C to 270 °C markedly promoted an increase in intrinsic viscosity. After 16 h, the intrinsic viscosity increased from 0.50 dL/g at 230 °C to 1.25 dL/g at 270 °C. However, prolonged treatment at elevated temperatures also led to visible yellowing of the polyamide, suggesting the occurrence of thermally induced side reactions, such as the thermal oxidation and cyclization of BDA.[36,37] Therefore, an SSP temperature of 270 °C and a reaction time of 8–16 h were appropriate for balancing the molecular weight growth and avoiding thermal degradation. For the MP of PA412, the intrinsic viscosity in-

https://doi.org/10.1007/s10118-026-3876-2

creased rapidly during the initial 2–4 h, and then increased gradually with further extension of the reaction time (Fig. 1b). Within the investigated temperature range, the increase in temperature led to only a slight enhancement in the intrinsic viscosity. Among the investigated conditions, MP at 280 °C resulted in the highest intrinsic viscosity and was therefore selected for the subsequent preparation of PA410 and PA412.

The optimized post-polycondensation conditions are listed in Table S1 (in the electronic supplementary information, ESI). For PA46 and PA48, stepwise heating could further promote intrinsic viscosities while avoiding prolonged exposure to high post-polycondensation temperatures. Compared with single-stage SSP, stepwise heating programs markedly increased the intrinsic viscosities of both polyamides. For PA46, the intrinsic viscosity increased from 1.25 dL/g after single-stage SSP at 270 °C for 16 h to 1.65–1.71 dL/g after stepwise SSP. Similarly, the intrinsic viscosity of PA48 increased from 0.70 dL/g after single-stage SSP at 240 °C to 1.16–1.29 dL/g after stepwise treatment. These results indicated that an appropriate temperature sequence could promote further chain extension more effectively than prolonged treatment at a single temperature. Accordingly, the PA46, PA48, PA410 and PA412 with high intrinsic viscosities of 1.65, 1.29, 1.32 and 1.47 dL/g, respectively, were selected for subsequent structural and property characterization.

The chemical structure of the synthesized PA4X was confirmed by ^{1}H-NMR spectroscopy, as shown in Fig. 2(A). For PA46, the signals at 4.03 ppm (peak a) and 3.20 ppm (peak c) were assigned to the α-CH_2 protons adjacent to the amine groups (NH) and carbonyl groups (C=O), respectively. The signals at 2.19 ppm (peak b) and 2.28 ppm (peak d) were attributed to the β-CH_2 protons relative to the NH and C=O groups, respectively. As *X* increased, the resonance associated with peak b gradually shifted upfield and increasingly overlapped with peak d. Meanwhile, the additional resonances appeared at 1.81 ppm (peak e) and 1.76 ppm (peak f), corresponding to the methylene protons located farther from the amide groups. ^{1}H-NMR results confirmed the successful synthesis of PA4X with distinct chain lengths. The thermal degradation behavior of PA4X was evaluated by TGA under a nitrogen atmosphere. As shown in Fig. 2(B), all the samples displayed a predominant single weight-loss step. The 5 wt%

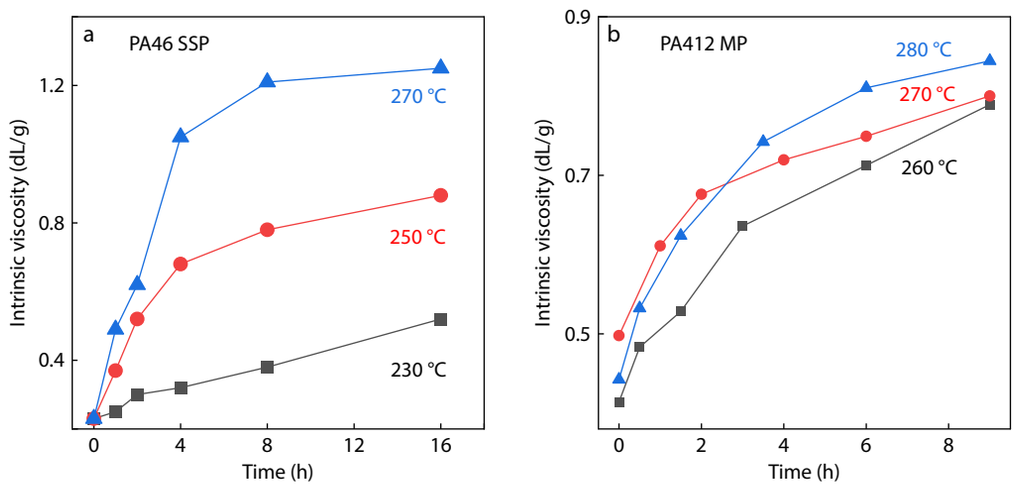


Fig. 1 Post-polycondensation kinetics of PA4X. Change of intrinsic viscosity with time during (a) solid-state post-polycondensation of PA46 and (b) melt post-polycondensation of PA412.

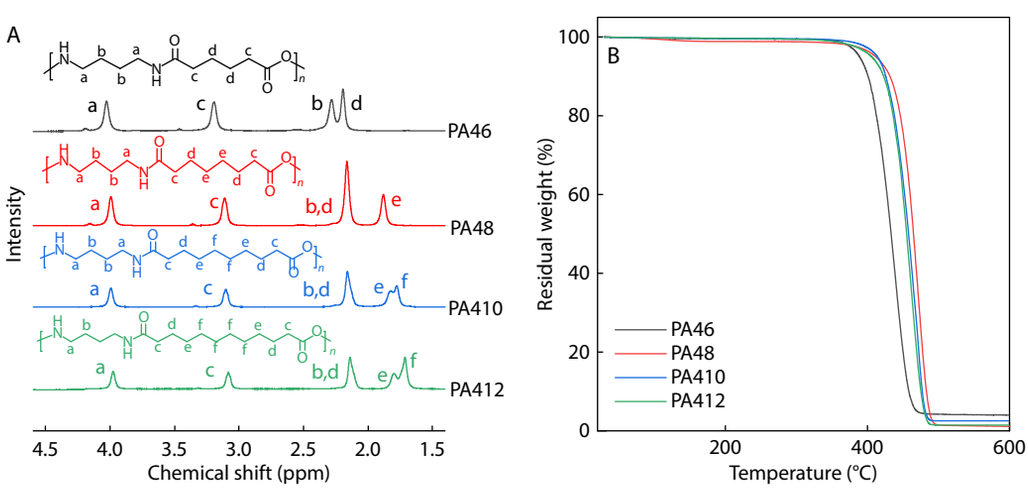


Fig. 2 (A) ^{1}H-NMR spectra and (B) TGA curves of PA4X.

https://doi.org/10.1007/s10118-026-3876-2

thermal degradation temperatures for all PA4X were higher than about 390 °C, demonstrating their high thermal stability, which also provided sufficient thermal stability for the subsequent melting and crystallization processes.

Nonisothermal Crystallization and Melting Behavior of Polyamides

We first investigated the non-isothermal crystallization and melting behavior of PA4X by DSC. Figs. 3(a) and 3(b) depict the DSC cooling and subsequent heating curves recorded at 10 °C/min, and Figs. 3(c) and 3(d) summarize the evolution of the melting (T_m) and crystallization temperatures (T_c), melting (ΔH_m), and crystallization enthalpies (ΔH_c) with X. As shown in Figs. 3(a) and 3(b), all PA4X samples exhibited obvious crystallization and melting peaks during cooling from the melt state and subsequent heating, respectively, confirming that they are crystallizable under cooling conditions. During the subsequent heating process, only PA412 exhibited an obvious cold crystallization peak before melting. This indicated that the crystallization of PA412 was incomplete during cooling, and the remaining amorphous chains underwent further crystallization upon heating. PA46 displayed the highest T_c of 262 °C, whereas the T_c values of PA48, PA410, and PA412 progressively decreased to 233, 222, and 210 °C (Fig. 3c), respectively. A corresponding decrease in T_m was observed, which decreased from 291 °C for PA46 to 240 °C for PA412 with increasing X (Fig. 3c).

As shown in Fig. 3(d), ΔH_m and ΔH_c have similar values and both decreased progressively with increasing X. For the PA4X series, increasing X reduces the density of amide groups and intermolecular H-bonds while enhancing the chain flexibility. The weakening of intermolecular interactions decreased the stability of the crystalline phase and thus retarded crystallization, leading to decreases in T_m, T_c, ΔH_m and ΔH_c. The DSC-derived crystallinity ($\omega_{c,DSC}$) of PA4X was calculated according to $\omega_{c,DSC} = \Delta H_m/\Delta H_m^0$, where ΔH_m is the measured melting enthalpy obtained from DSC results, and ΔH_m^0 is the equilibrium melting enthalpy of the corresponding 100% crystalline polyamide. The ΔH_m^0 values of PA4X were estimated using Van Krevelen's group contribution method (Table S2 in ESI). $\omega_{c,DSC}$ of PA4X decreased from 41.2% for PA46 to 21.1% for PA412 as X increased from 6 to 12. The higher crystallinity of PA4X with smaller X was primarily attributed to its higher amide-group density, which facilitated closer chain packing and the formation of a dense and stable intermolecular H-bonding network.

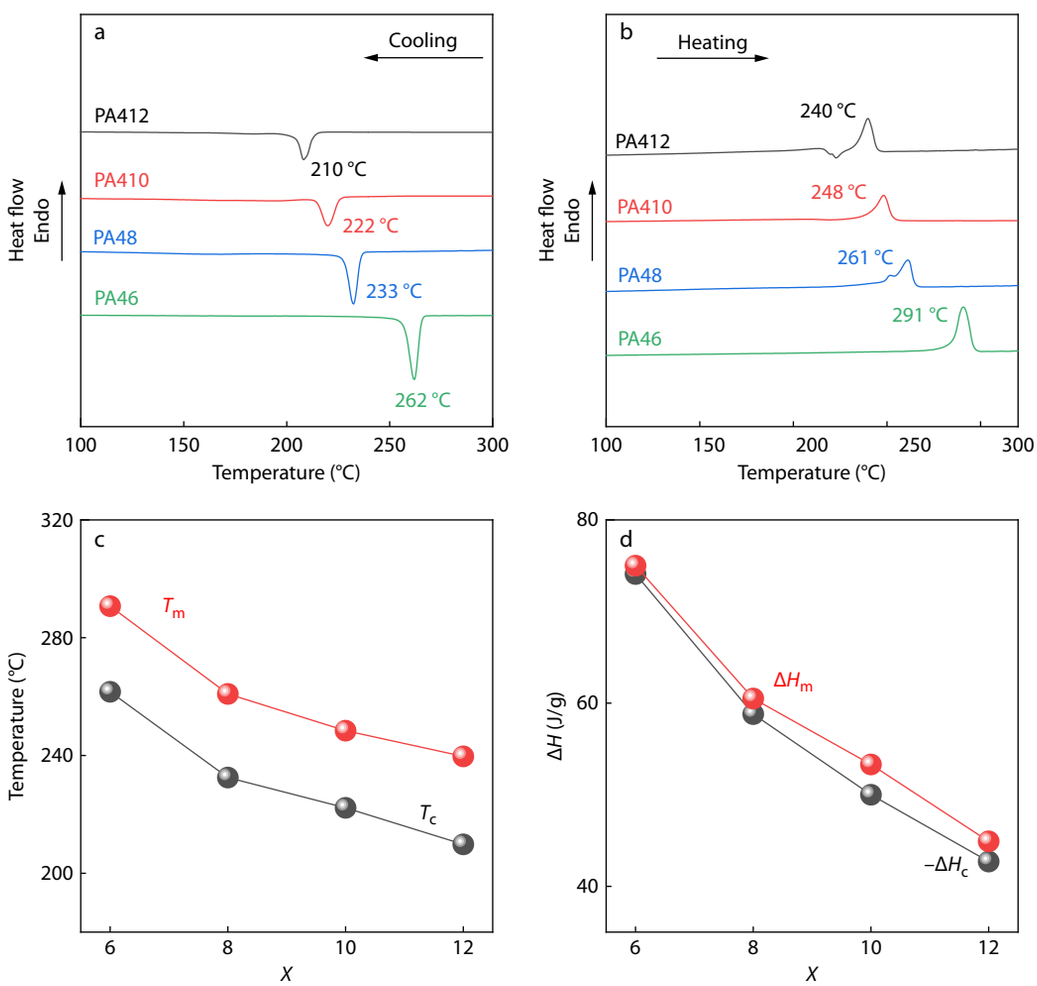


Fig. 3 Nonisothermal crystallization and melting behavior of PA4X. DSC curves collected upon (a) cooling from the melt and (b) subsequent heating; Evolutions of (c) T_c, T_m and (d) ΔH_c, ΔH_m with X.

https://doi.org/10.1007/s10118-026-3876-2

Crystalline Structures of Polyamides

The crystalline structures of the solution- and melt-crystallized PA4X samples were further investigated using WAXS. The solution-crystallized samples were obtained by crystallization from formic acid and the melt-crystallized samples were prepared by isothermal melt crystallization at 200 °C. Fig. 4 shows the WAXS results for solution-crystallized PA4X samples. As shown in Fig. 4(a), all PA4X samples exhibited three characteristic diffraction peaks, which were assigned to the (002), (100), and (010/110) planes of the triclinic α phase of common polyamides.[38,39] This suggests that the solution-crystallized PA4X samples mainly formed a triclinic α phase in formic acid. The positions of the (100) and (010/110) reflections remained nearly unchanged as X varied, whereas the (002) reflection progressively shifted to a lower q value. This shift indicated an increase in the corresponding lattice spacing as the methylene segment became longer. According to Bragg's equation (d=2π/q), the lattice spacings of each diffraction plane [$d_{\alpha(100)}$, $d_{\alpha(010/110)}$ and $d_{\alpha(002)}$] were calculated and plotted against X in Fig. 4(b). As shown in Fig. 4(b), $d_{\alpha(100)}$ and $d_{\alpha(010/110)}$ of all PA4X remained nearly constant at 0.44 and 0.37 nm, respectively. However, $d_{\alpha(002)}$ increased gradually from 0.53 nm to 0.86 nm with increasing X from 6 to 12. The (100) and (010/110) reflections correspond to the interchain distance within the H-bonded sheets and intersheet distance, respectively. Because both reflections primarily reflect lateral chain packing, their positions are almost unchanged with the change in repeat-unit length.[39,40] However, the (002) plane is associated with periodicity along the chain-axis direction, which increases with the methylene segment length.

Fig. 5(a) shows that the PA4X samples melt-crystallized at 200 °C and measured at 25 °C mainly formed an α phase. An additional weak diffraction peak at 15.2 nm^{-1}, located between the (100) and (010/110) diffraction peaks, was observed for melt-crystallized PA412, indicating the predominance of the α phase with a small fraction of the γ phase.[39] The WAXS-derived crystallinity ($\omega_{c,WAXS}$) of the melt-crystallized samples was estimated by the peak splitting and fitting

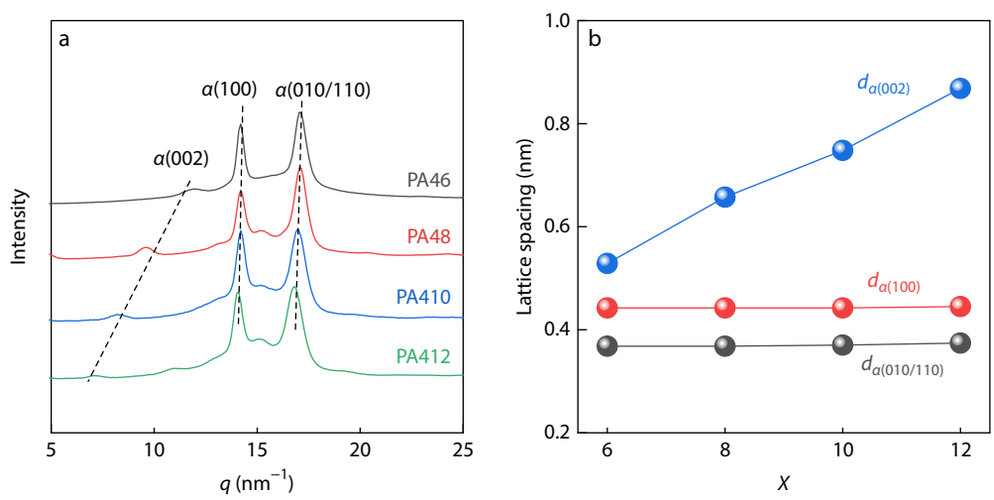


Fig. 4 Crystalline structure of solution-crystallized PA4X. (a) WAXS profiles; (b) Change of lattice spacing with X derived from panel a. All measurements were conducted at 25 °C.

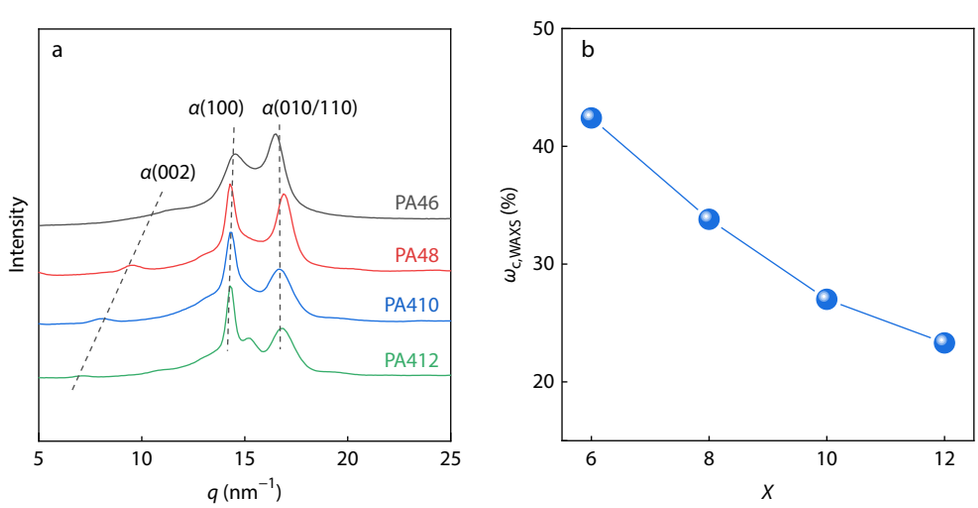


Fig. 5 Crystalline structure of melt-crystallized PA4X at 25 °C. (a) WAXS profiles; (b) Evolution of $\omega_{c,WAXS}$ with X calculated by peak splitting and fitting of WAXS profiles in panel a. All measurements were conducted at 25 °C.

https://doi.org/10.1007/s10118-026-3876-2

of the WAXS profiles (Fig. S1 in ESI). As shown in Fig. 5(b), $\omega_{c,WAXS}$ decreased gradually with increasing X, which was consistent with the trend obtained from the DSC results. Specifically, as X increased from 6 to 12, $\omega_{c,WAXS}$ gradually declined from 42.4% to 23.3%. This is because extending the methylene segment length reduces the amide-group density and weakens the intermolecular H-bonding, thereby reducing the ability of the PA4X chains to organize into a highly ordered crystalline structure.

Crystalline Phase Transitions of Polyamides upon Heating and Cooling

Temperature-variable WAXS measurements were employed to investigate the crystalline phase transition of solution-crystallized PA4X during heating and subsequent cooling processes. The samples were heated from 25 °C to the melted state at 5 °C/min and then cooled to 25 °C. As shown in Figs. 6(a)–6(d), all PA4X samples initially exhibited the (100) and (010/110) reflections of the triclinic α phase before heating. For PA46 in Fig. 6(a), the characteristic diffraction peaks of triclinic α phase gradually approached each other with increasing temperature and merged into a single peak at q=15.0 nm^{-1}, which corresponds to the pseudohexagonal γ phase.[39] This indicated a transformation from the triclinic α phase to the pseudohexagonal γ phase upon heating, which is a typical behavior of the Brill transition in polyamides.[22] The corresponding temperatures of the (100) and (010/110) diffraction merging are defined as T_B, as indicated by the dark blue curves in Fig. 6. Upon further heating to 253 °C, the γ-phase reflection disappeared owing to crystal melting. A similar α-to-γ transition was observed for PA48, PA410, and PA412 upon heating (Figs. 6b–6d).

The temperature dependences of the corresponding lattice spacings were evaluated and plotted in Fig. 6(e) and Fig. S2 (in ESI). During heating, the $d_{\alpha(100)}$ value gradually decreased, whereas the $d_{\alpha(010/110)}$ value increased markedly. The two lattice spacings converged at T_B, and the corresponding T_B values were plotted against X in Fig. 6(f). Notably, T_B decreased progressively from 253 °C for PA46 to 227, 217 and 203 °C for PA48, PA410 and PA412, respectively, as X increased from 6 to 12. The decrease in T_B is closely associated with the progressive reduction in the amide-group density and the corresponding weakening of the intermolecular H-bonding network as the methylene sequence became longer.[41] As previously reported,[25] a more ordered and stable H-bonded framework requires a higher temperature to undergo Brill transition. In the PA4X series, PA46 possesses a denser and more ordered H-bonding network than PA412 and consequently exhibited a substantially higher T_B. Moreover, previous studies demonstrated that T_B is positively correlated with increasing lamellar thickness (L_c).[22,42] The slight decrease in L_c with increasing X may also have contributed to the observed decrease in T_B, together with the effects of the chain structure and H-bond organization (Fig. S3 in ESI).

The crystalline phase transition of PA4X during cooling from the melt state to 25 °C was also investigated using temperature-variable WAXS, as shown in Fig. S4 (in ESI). For all the PA4X samples, the pseudohexagonal γ phase formed at the initial stage of crystallization, and its diffraction progressively

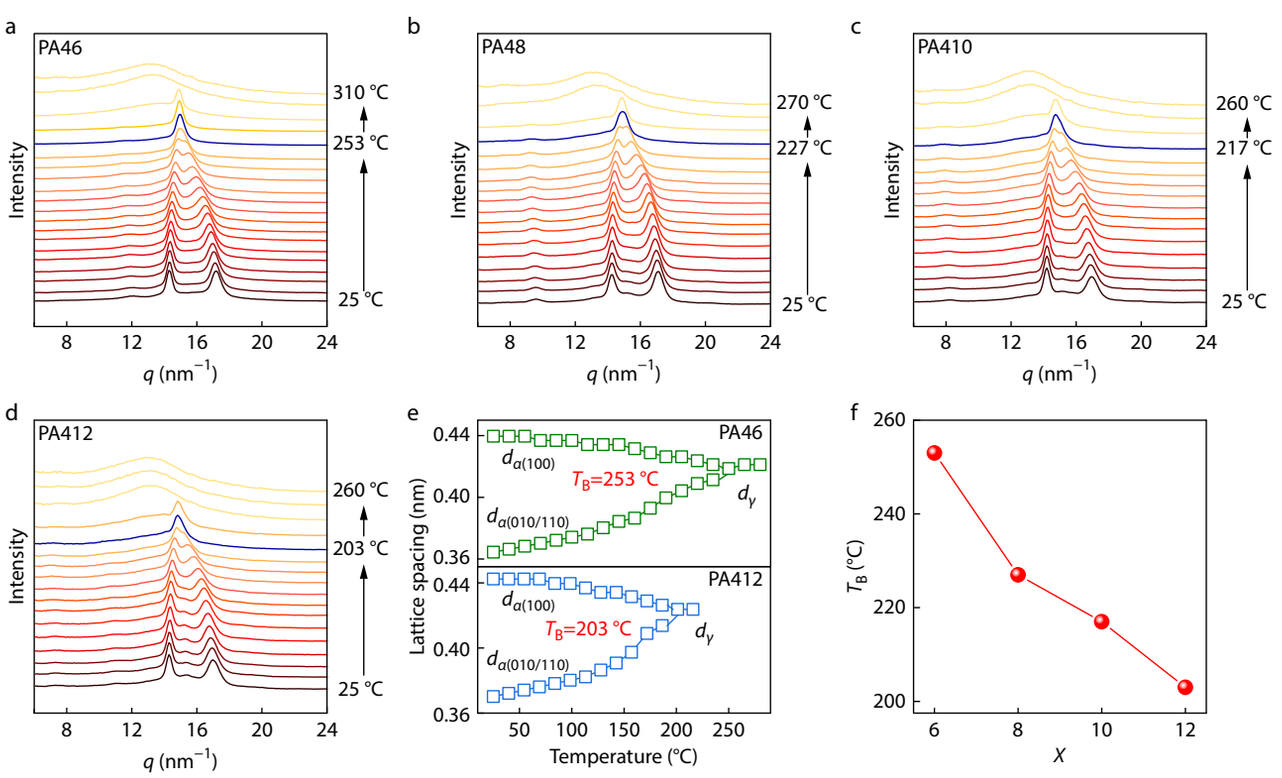


Fig. 6 Temperature-variable WAXS profiles of solution-crystallized PA4X collected upon heating from 25 °C to the melt state at 5 °C/min. (a) PA46, (b) PA48, (c) PA410 and (d) PA412; (e) Evolutions of lattice spacing with temperature for PA46 and PA412; (f) Evolution of Brill transition temperature with X. The dark blue lines in panels a–d indicate the Brill transition temperature.

https://doi.org/10.1007/s10118-026-3876-2

intensified upon cooling. At lower temperatures, this reflection split into the characteristic (100) and (010/110) reflections of the triclinic *α* phase, demonstrating a reversible *γ*-to-*α* transition. The *α*-phase reflections observed during cooling from the melt state were less widely separated than those of the initial solution-crystallized samples, suggesting a lower degree of crystal perfection in the melt-crystallized *α* phase. The reduced T_B of *γ*-to-*α* transition for PA46 upon cooling was likely associated with its relatively less perfect *α*-phase packing, together with the contribution from the lamellar thickness. Overall, the temperature-variable WAXS results demonstrated that all PA4X undergo a reversible *α*-*γ* Brill transition during the heating and cooling cycles.

Mechanical Property and Water Absorption

Mechanical properties of PA4X were evaluated by uniaxial tensile testing, and the corresponding engineering stress-strain curves are shown in Fig. 7(a). All the samples exhibited the typical deformation behavior of semicrystalline thermoplastics, including the stages of elastic deformation, yielding, necking, and strain hardening. The PA4X samples exhibited a gradual transition from a relatively stiff material to a ductile one. The yield stress, Young's modulus, and strain at break of the PA4X are summarized in Figs. 7(b)–7(d). PA46 exhibited the highest yield stress (59.2 MPa) and Young's modulus (1152 MPa) and a strain at break of 60.3%. Both the yield stress and Young's modulus decreased progressively, while the strain at break increased markedly with greater *X*. Specifically, as *X* increased from 6 to 12, the yield stress and Young's modulus decreased from 59.2 MPa to 38.2 MPa and 1152 MPa to 537 MPa, respectively, while the strain at break increased from 60.3% to 246%. The higher ductility of PA4X with a greater *X* is primarily attributed to the lower crystallinity, weaker intermolecular H-bonding interactions, and high chain mobility. Therefore, PA4X possesses a tunable balance between stiffness, strength, and ductility by varying the methylene sequence length in the diacid units.

Water absorption is an important factor for the service stability of polyamides. The amide groups along the molecular chains can form H-bonds with water molecules, leading to water uptake and the possible plasticization of the polymer matrix. Fig. 8(a) shows that the water absorption of all the PA4X samples increased rapidly during the initial immersion stage and then gradually approached an equilibrium value. As shown in Fig. 8(b), the equilibrium water absorption decreased from 10.5% for PA46 to 3.7% for PA412 as *X* increased from 6 to 12. This pronounced reduction in water ab-

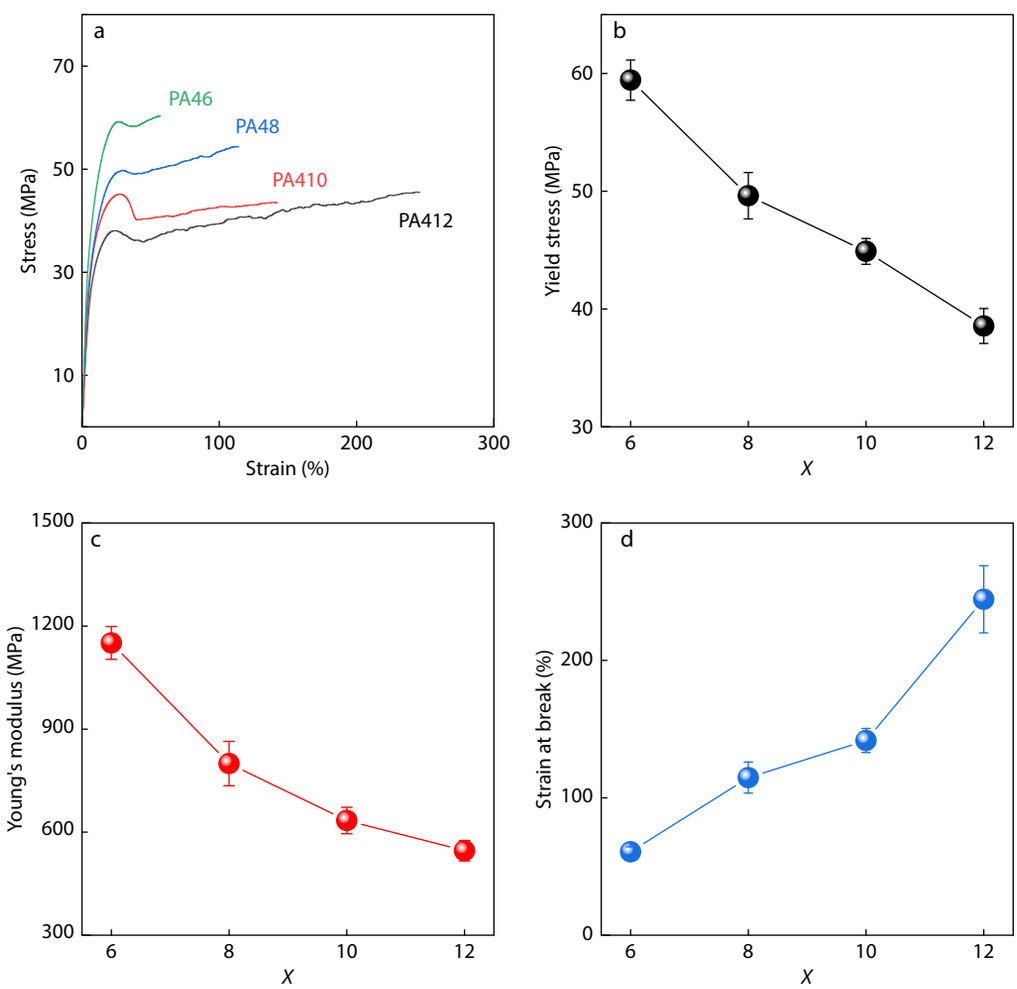


Fig. 7 Mechanical properties of PA4X. (a) Engineering stress-strain curves, (b) yield stress, (c) Young's modulus, and (d) strain at break.

https://doi.org/10.1007/s10118-026-3876-2

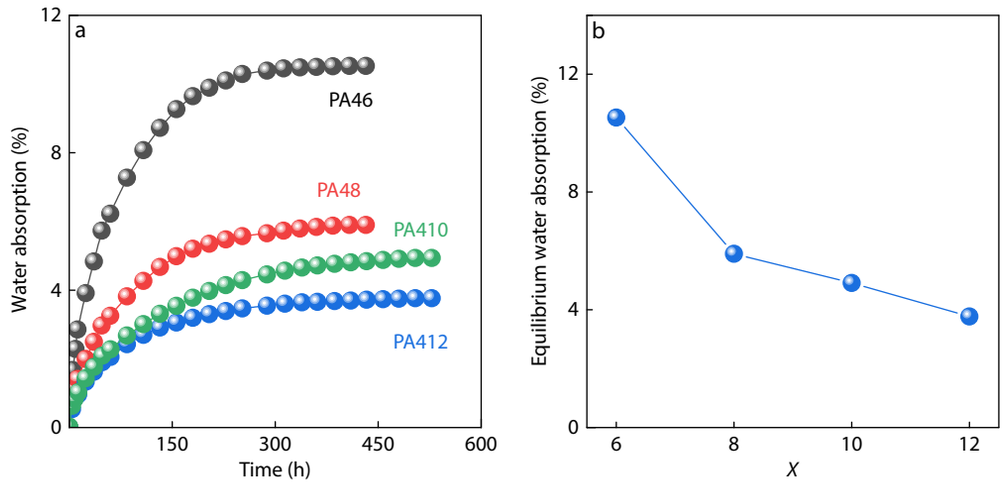


Fig. 8 Water absorption of PA4X. (a) Evolutions of water absorption with immersion time, and (b) equilibrium water absorption.

sorption was mainly ascribed to the decreasing concentration of polar amide groups as the methylene sequence lengthened. The lower density of the amide groups reduces the number of accessible H-bonding sites for water molecules, thereby suppressing water uptake. Notably, the water absorption decreased despite the reduction in crystallinity with greater *X*, indicating that the variation in the amide-group density exerted a stronger influence on water uptake than the crystallinity. Thus, increasing the methylene sequence length in the diacid units not only enhances the ductility but also improves the resistance to water absorption, although at the expense of stiffness and yield strength.

CONCLUSIONS

In summary, high-molecular-weight PA4X with various methylene sequence lengths was successfully prepared through aqueous prepolymerization, followed by either solid-state or melt post-polycondensation. The T_c, T_m, enthalpies, and crystallinity of PA4X progressively decreased with increasing *X* because of the reduced amide-group density and weakened intermolecular H-bonding networks. The solution-crystallized samples mainly formed the triclinic *α* phase and underwent an *α*-*γ* Brill transition upon heating, with T_B being greatly dependent on the methylene sequence length. T_B decreased from 253 °C for PA46 to 203 °C for PA412 as *X* increased from 6 to 12. Upon cooling from the melt state, a reversible *γ*-to-*α* transition occurred in all PA4X. The increase in *X* resulted in a lower yield stress and Young's modulus but markedly enhanced ductility and reduced water absorption. In particular, PA412 exhibited a strain at break of 246% and an equilibrium water absorption of 3.7%. This work elucidates the role of the methylene sequence length in the crystallization, phase transition, and physical performance of PA4X, and provides a molecular-level basis for designing bio-based polyamides with tunable structures and performances.

Conflict of Interests

The authors declare no interest conflict.

Electronic Supplementary Information

Electronic supplementary information (ESI) is available free of charge in the online version of this article at http://doi.org/10.1007/s10118-026-3876-2.

Data Availability Statement

The data that support the findings of this study are available from the corresponding author upon reasonable request.

ACKNOWLEDGMENTS

This work was financially supported by the National Natural Science Foundation of China (No. U25B2098), Zhejiang Provincial Natural Science Foundation of China (No. LQZSZ25E030002), Fundamental and Interdisciplinary Disciplines Breakthrough Plan of the Ministry of Education of China (No. JYB2025XDXM407), and the State Key Laboratory of Chemical Engineering and Low-Carbon Technology (No. SKL-ChE-26T05).

REFERENCES

1 Wang, Y.; Yang, C.; Guo, B.; Kuang, T.; Liu, Y.; He, M.; Qin, S.; Yu, J. Biobased polyamide 5652 with *α*-crystal form: characterization and low moisture absorption. *Macromolecules* **2025**, *58*, 7323–7333.
2 Marchildon, K. Polyamides–still strong after seventy years. *Macromol. React. Eng.* **2011**, *5*, 22–54.
3 Lee, J. A.; Kim, J. Y.; Ahn, J. H.; Ahn, Y. J.; Lee, S. Y. Current advancements in the bio-based production of polyamides. *Trends Chem.* **2023**, *5*, 873–891.
4 Winnacker, M.; Rieger, B. Biobased polyamides: recent advances in basic and applied research. *Macromol. Rapid Commun.* **2016**, *37*, 1391–1413.
5 Gong, S.; Zhao, S.; Tang, J.; Chen, X.; Zhao, B.; Ren, C.; Zhao, Z.; Pan, K. Biobased polyamides: monomer sources, preparation, functional modifications, and applications. *Macromol. Rapid Commun.* **2025**, *46*, 2500197.
6 Zhu, Y.; Romain, C.; Williams, C. K. Sustainable polymers from renewable resources. *Nature* **2016**, *540*, 354–362.

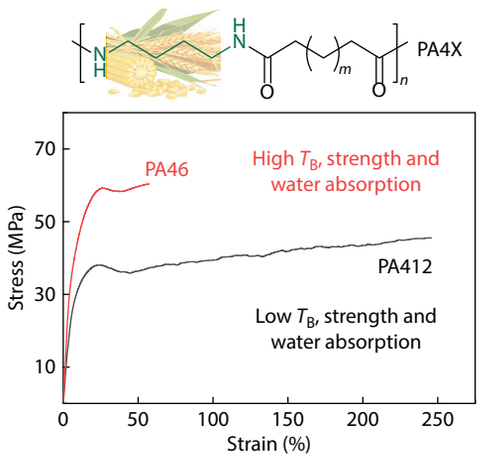
Graphical Abstract

Crystallization, Brill Transition, and Physical Properties of Biobased 1,4-Butanediamine-derived Polyamides Controlled by Methylene Sequence Length

Jun-Jian Qiu, Ying Zheng, Mao-Lin Li, Chang Zeng, Feng Zhou, Xian-Ming Li, Ke-Yuan Liu, Jun-Feng Liu, Cheng-Tao Yu, and Peng-Ju Pan

Polytechnic Institute of Zhejiang University; Zhejiang University; SINOPEC Dalian Research Institute of Petroleum and Petrochemicals Co., Ltd.; Jiangsu Qingquan Chemical Co., Ltd.

Biobased PA4X polyamides were synthesized from 1,4-diaminobutane and aliphatic diacids of various chain lengths. Shorter-chain PA4X exhibits a higher Brill-transition temperature, strength, and water absorption, whereas the longer-chain analogs show a lower Brill-transition temperature, strength, and reduced water absorption.



Chinese J. Polym. Sci. 2026 *https://doi.org/10.1007/s10118-026-3876-2*

7 Tao, L.; Liu, K.; Li, T.; Xiao, R. Preparation and properties of biobased polyamides based on 1,9-azelaic acid and different chain length diamines. *Polym. Bull.* **2020**, *77*, 1135–1156.
8 Xie, S.; Yu, D.; Yao, J.; Wei, Z.; Wang, X.; Yang, J. Synthesis of biobased furan polyamides with excellent mechanical properties: effect of diamine chain length. *J. Polym. Environ.* **2024**, *32*, 3195–3207.
9 Zhu, R.; Hu, H.; Sun, L.; Zhao, R.; Ma, B.; Li, N.; Yu, J.; Wang, X.; Cheng, L. Tunable crystallization behavior, memory effect, and thermo-mechanical properties of biobased polyamides PA5X. *Polymer* **2024**, *313*, 127687.
10 Nguyen, P. H.; Spoljaric, S.; Seppälä, J. Redefining polyamide property profiles *via* renewable long-chain aliphatic segments: towards impact resistance and low water absorption. *Eur. Polym. J.* **2018**, *109*, 16–25.
11 Xia, J.; Ni, L.; Sun, C.; Zheng, Y.; Liu, J.; Yu, C.; Li, W.; Wang, J.; Pan, P. Crystal polymorphism and phase transition of isodimorphic copolyamides based on even–even and odd–even comonomer units: synergistic effects of copolymer composition and crystallization temperature. *Macromolecules* **2024**, *57*, 2835–2847.
12 Pérez-Camargo, R. A.; Torres, J.; Müller, A. J. Understanding even-odd effects in linear semi-crystalline polymers: polyethers, polycarbonates, polyesters, and polyamides. *Polymer* **2025**, *324*, 128233.
13 Du, M.; Jariyavidyanont, K.; Schick, C.; Androsch, R. Physical aging and Young's modulus of polyamide 11 containing different crystal polymorphs. *Macromol. Mater. Eng.* **2025**, *310*, e00242.
14 Ramesh, C. New crystalline transitions in nylons 4, 6, 6, 10, and 6, 12 using high temperature X-ray diffraction studies. *Macromolecules* **1999**, *32*, 3721–3726.
15 Jones, N. A.; Atkins, E. D. T.; Hill, M. J. Investigation of solution-grown, chain-folded lamellar crystals of the even-even nylons: 6 6, 8 6, 8 8, 10 6, 10 8, 10 10, 12 6, 12 8, 12 10, and 12 12. *J. Polym. Sci. B Polym. Phys.* **2000**, *38*, 1209–1221.
16 Villaseñor, P.; Franco, L.; Subirana, J. A.; Puiggalí, J. On the crystal structure of odd-even nylons: polymorphism of nylon 5, 10. *J. Polym. Sci. B Polym. Phys.* **1999**, *37*, 2383–2395.
17 An, M.; Zhang, Q.; Lin, Y.; Wang, D.; Chen, W.; Meng, L.; Yin, P.; Li, L. Stretch-induced reverse Brill transition in polyamide 46. *Macromolecules* **2020**, *53*, 11153–11165.
18 Chen, Y. H.; Chang, Y. C.; Rwei, S. P. High-value copolyamide 6 materials with colorless transparent and low water absorption upgraded from upcycled and biomass comonomers. *Polymer* **2022**, *257*, 125269.
19 Morales-Gámez, L.; Soto, D.; Franco, L.; Puiggalí, J. Brill transition and melt crystallization of nylon 56: an odd–even polyamide with two hydrogen-bonding directions. *Polymer* **2010**, *51*, 5788–5798.
20 Yoshioka, Y.; Tashiro, K.; Ramesh, C. Structural change in the Brill transition of nylon m/n (2) conformational disordering as viewed from the temperature-dependent infrared spectral measurements. *Polymer* **2003**, *44*, 6407–6417.
21 Kang, H.; Wang, Z.; Hao, X.; Liu, R. Thermal induced crystalline transition of bio-based polyamide 56. *Polymer* **2022**, *242*, 124540.
22 Lotz, B. Brill transition in nylons: the structural scenario (#). *Macromolecules* **2021**, *54*, 565–583.
23 Xia, J.; Xu, S.; Zheng, Y.; Zhou, J.; Yu, C.; Shan, G.; Bao, Y.; Pan, P. Isodimorphic crystallization and tunable γ–α phase transition in aliphatic copolyamides: critical roles of comonomer defects and conformational evolution. *Macromolecules* **2022**, *55*, 6090–6101.
24 Sattler, R.; Danke, V.; Beiner, M. Long chain polyamides: influence of methylene sequence length and external forces on structural features. *Macromol. Chem. Phys.* **2023**, *224*, 2200433.
25 Wang, Y.; Zhu, P.; Qian, C.; Zhao, Y.; Wang, L.; Wang, D.; Dong, X. The Brill transition in long-chain aliphatic polyamide 1012: the role of hydrogen-bonding organization. *Macromolecules* **2021**, *54*, 6835–6844.
26 Pepin, J.; Miri, V.; Lefebvre, J. M. New insights into the Brill transition in polyamide 11 and polyamide 6. *Macromolecules*

2016, *49*, 564–573.
27 Ding, M.; Ni, L.; Xia, J.; Zheng, Y.; Yu, C.; Shan, G.; Bao, Y.; Pan, P. Linearly-changed thermal behavior and depressed Brill transition in long-chain polyamides substituted by methyl side groups. *ACS Macro Lett.* **2024**, *13*, 354–360.
28 Zhang, X.; Buzinkai, J.; Androsch, R.; Colby, R. H.; Rhoades, A. M. Crystallization of polyamide 66 in blends with a random noncrystallizable poly(hexamethylene isophthalamide-*co*-terephthalamide). *Macromolecules* **2025**, *58*, 8151–8164.
29 Qian, Z. G.; Xia, X. X.; Lee, S. Y. Metabolic engineering of escherichia coli for the production of putrescine: a four carbon diamine. *Biotechnol. Bioeng.* **2009**, *104*, 651–662.
30 Ren, Y.; Celińska, E.; Cai, P.; Zhou, Y. J. Combing directed enzyme evolution with metabolic engineering to develop efficient microbial cell factories. *Chem. Bio. Eng.* **2025**, *2*, 449–459.
31 Wang, X.; Gao, S.; Wang, J.; Xu, S.; Li, H.; Chen, K.; Ouyang, P. The production of biobased diamines from renewable carbon sources: current advances and perspectives. *Chin. J. Chem. Eng.* **2021**, *30*, 4–13.
32 Gaymans, R. J.; Van Utteren, T. E. C.; Van Den Berg, J. W. A.; Schuyer, J. Preparation and some properties of nylon 46. *J. Polym. Sci. Polym. Chem. Ed.* **1977**, *15*, 537–545.
33 Zhang, Z.; Huang, K.; Liu, Z. Synthesis of high molecular weight nylon 46 in supercritical carbon dioxide. *Macromolecules* **2011**, *44*, 820–825.
34 Moran, C. S.; Barthelon, A.; Pearsall, A.; Mittal, V.; Dorgan, J. R. Biorenewable blends of polyamide-4,10 and polyamide-6,10. *J. Appl. Polym. Sci.* **2016**, *133*, 43626.
35 Safari, M.; Otaegi, I.; Aramburu, N.; Wang, Y.; Liu, G.; Dong, X.; Wang, D.; Guerrica-Echevarria, G.; Müller, A. J. Composition dependent miscibility in the crystalline state of polyamide 6/polyamide 4, 10 blends: from single to double crystalline blends. *Polymer* **2021**, *219*, 123570.
36 Roerdink, E.; Warnier, J. M. M. Preparation and properties of high molar mass nylon-4, 6: a new development in nylon polymers. *Polymer* **1985**, *26*, 1582–1588.
37 Srinivasan, R.; Almonacil, C.; Narayan, S.; Desai, P.; Abhiraman, A. S. Mechanism, kinetics and potential morphological consequences of solid-state polymerization. *Macromolecules* **1998**, *31*, 6813–6821.
38 Atkins, E. D. T.; Hill, M.; Hong, S. K.; Keller, A.; Organ, S. Lamellar structure and morphology of nylon 46 crystals: a new chain folding mechanism for nylons. *Macromolecules* **1992**, *25*, 917–924.
39 Jones, N. A.; Atkins, E. D. T.; Hill, M. J.; Cooper, S. J.; Franco, L. Chain-folded lamellar crystals of aliphatic polyamides. Investigation of nylons 4 8, 4 10, 4 12, 6 10, 6 12, 6 18 and 8 12. *Polymer* **1997**, *38*, 2689–2699.
40 Bermúdez, M.; León, S.; Alemán, C.; Muñoz-Guerra, S. Structure and morphology of nylon 46 lamellar crystals: electron microscopy and energy calculations. *J. Polym. Sci. B Polym. Phys.* **2000**, *38*, 41.
41 Vinken, E.; Terry, A. E.; Hoffmann, S.; Vanhaecht, B.; Koning, C. E.; Rastogi, S. Influence of hydrogen bonding on the conformational changes, the Brill transition, and lamellae thickening in (co)polyamides. *Macromolecules* **2006**, *39*, 2546–2552.
42 Yang, X.; Tan, S.; Li, G.; Zhou, E. Dependence of the Brill transition on the crystal size of nylon 10 10. *Macromolecules* **2001**, *34*, 5936–5942.

https://doi.org/10.1007/s10118-026-3876-2